Final state interaction in (³He,²He) reactions

T. V. Congedo, I. S. Lee-Fan, and B. L. Cohen

University of Pittsburgh, Pittsburgh, Pennsylvania 15260

(Received 8 February 1980)

The two protons from ²He breakup following (³He,²He) reactions were detected in coincidence, and energy and angular correlations between them were studied and compared with predictions of the final state interaction theories of Watson and Migdal and Phillips, Griffy, and Biedenharn. The angular correlation between the breakup protons drops off much faster than predicted by these theories; a final state interaction empirically derived to fit the angular correlation is sharply peaked at a breakup energy ≈0.6 MeV and is quite narrow. Energy distributions of the protons have a dip at the center for small correlation angles which disappears at larger angles. This is well predicted by all final state interaction theories but the slopes of these distributions are much better fit by the empirical final state interaction than by Watson and Migdal or by Phillips, Griffy, and Biedenharn. By maintaining a constant small correlation angle (proton detectors close together), ²He angular distributions were measured and found to be in good agreement with distorted-wave Born approximation predictions.

I. INTRODUCTION

In nuclear reactions, the emission of any particle (i.e., nucleus) in any quantum state has equal *a priori* probability (its actual probability of emission is determined by statistical considerations of density of final states). In many cases, these particles may be unstable and decay rapidly but this represents no complication if the half-life is not extremely short; for example, ^{8}Be particles which have a half-life of 3×10^{-16} sec have been used[1] and present little difficulty in analysis or even in experimental detection.

For reaction products with extremely short half-lives, however, there are complications. Two of the simplest examples of this type are the deuteron in the singlet state and the ^{2}He nucleus. The former has been studied previously,[2] and in this paper we study the latter, which rapidly decays into two protons. One immediate problem from the short half-life here is that, due to the uncertainty principle, the energy of the ^{2}He nucleus emerging from the nuclear reaction is not well defined. It is largely this problem which is confronted here. The difficulties would be much further compounded if the half-life were so short that the decay takes place during the course of the nuclear reaction, and one of the goals of this paper is to determine the importance of that possible complication.

If we ignore the latter complication, the reaction can be thought of as taking place in two independent steps: first a nuclear reaction in which a ^{2}He nucleus is produced and emerges, and sec-

ond, a subsequent decay of the ^{2}He. In the (^{3}He, ^{2}He) reaction used in these studies, the first process should be understandable in terms of neutron transfer reaction theory commonly treated with distorted-wave–Born-approximation (DWBA) calculations. The second step is commonly referred to as the "final state interaction" (FSI) and should be understandable in terms of the interaction between two protons as determined from proton-proton scattering experiments. If this separation into two steps is valid, each step can not only be calculated separately but they can be separately tested experimentally. The principal purpose of this paper is to carry out these experimental tests.

Experimentally, a ^{2}He nucleus can only be detected by coincidence detection of the two protons into which it decays. By measuring their energies, E_1 and E_2, we can determine the Q value of the nuclear reaction in which the ^{2}He was produced from conservation of energy, as

$$E_1 + E_2 = E_{\text{inc}} + Q - E_{\text{rec}} , \qquad (1)$$

where E_{inc} is the energy of the incident particle which initiates the nuclear reaction, a ^{3}He particle in the (^{3}He, ^{2}He) reaction studied here, and E_{rec} is the recoil energy of the residual nucleus, calculable from kinematics for any known Q value. For the heavy target nuclei used in the studies reported here, E_{rec} is quite small and it will be ignored in qualitative introductory discussions, although it is used in all actual detailed calculations. The Q value of the reaction determines the final state of the residual nucleus which pro-

vides the information needed in the DWBA calculation for the first step. Note that $(E_1 + E_2)$ is a conserved quantity, unaffected by the uncertainty principle; it is related to the unconserved ^{2}He energy E_{He} by

$$E_{He} + E_{BU} = E_1 + E_2 , \qquad (2)$$

where E_{BU} is the energy in the breakup, the energy of the two protons relative to the center of mass motion of the ^{2}He. The fluctuations of E_{He}, referred to above as arising from the uncertainty principle, can therefore be represented by a probability distribution for E_{BU}, $\mathcal{P}(E_{BU})$, through (2). The theory of the final-state interaction has been treated by Watson,[3] Migdal,[4] and by Phillips, Griffy, and Biedenharn,[5] and they effectively give expressions for $\mathcal{P}(E_{BU})$ which are plotted in Fig. 1. According to (2), apart from a reversal and shift of the abscissa scale, this is the energy distribution of E_{He}; we see that it is indeed a broad distribution.

The two basic geometric variables in the reaction are θ, the angle between the directions of the incident ^{3}He and the emerging ^{2}He particles, and η, the angle between the two protons finally emitted. Since the ^{2}He particle is not directly observed, one cannot in general determine θ. However, if both protons are observed in the $\theta = 90°$ plane, it is kinematically required that the motion of the ^{2}He particle be in that plane. Because of this simplification, many of our measurements were

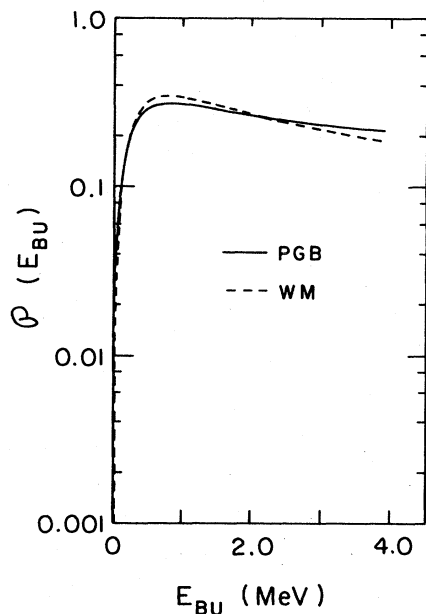FIG. 1. $\mathcal{P}(E_{BU})$ according to Phillips-Griffy-Biedenharn (solid curve) and Watson-Migdal (dashed curve). These are referred to as the final state interaction.

made at $\theta = 90°$, varying η within it, which allows us to study the second step of the process, breakup of the ^{2}He, while keeping all factors associated with the first step constant.

Measurements of that type then give the probability distribution of E_1, $P(E_1)$, for various η [note from (1) that $P(E_2)$ is completely equivalent, differing only by a reversal and shift of the abscissa scale]. Since the first step of the reaction, the (^{3}He, ^{2}He) neutron transfer, produces only a dependence on θ for a given transition (i.e., for a given Q value and hence for a given $E_1 + E_2$) and since θ is held constant at $90°$ for these measurements, the shape of $P(E_1)$ for various η is determined only by the second step of the reaction, the ^{2}He breakup. In fact, for any η, $P(E_1)$ is completely calculable from the information given.

To show this, consider the two proton detectors at a given angular separation in the $\theta = 90°$ plane, set to detect events in time coincidence with a given value of $E_1 + E_2$ determined by the known Q value of the reaction. A ^{2}He particle has equal probability of being emitted in any direction within the $\theta = 90°$ plane so we give each direction equal weight. For a given ^{2}He direction, the probability of a given distribution of the total available energy $E_{inc} + Q$ between E_{BU} and E_{He} is determined by Fig. 1. For a given E_{BU} and E_{He}, the energies and directions of the two emerging protons are determined by the polar and azimuthal angles between the velocity vector of the ^{2}He and the line of the opposing velocity vectors of the breakup in the center of mass system of the ^{2}He. Since directions between these velocity vectors are equally likely, all are given equal weight per unit solid angle. For a given case, one can apply vector addition to the velocities to determine the energies of the two protons, E_1 and E_2, and whether each strikes its respective detector. By cycling through all of the above mentioned variables (plus another associated with finite geometry in accepting small deviations from $\theta = 90°$) and accumulating all cases for which detection is achieved, one determines $P(E_1)$ from theory. This may be compared with measurements of $d^3\sigma/d\Omega_1 d\Omega_2 dE_1$, which should be proportional to $P(E_1)$. The process can be repeated for various η to determine the variation of $P(E_1)$ with η; and of course the integral under the curves $\int P(E_1) dE_1$ can be plotted vs η and compared with the results of the corresponding experimental procedures which give $d^2\sigma/d\Omega_1 d\Omega_2$. These two comparisons give an elaborate series of tests of the second step of the reaction, the ^{2}He breakup. The extent to which theory and experiment come together gives an indication of whether our original assumption of a two step process is acceptable.

In order to study the first step, the (^{3}He,^{2}He) reaction, one can take advantage of the fact that for small η, only a limited range of θ values is involved. In particular, if the plane including the target point and the two detectors is perpendicular to the plane of increasing θ through the midpoint between the two detectors, it is readily shown by solid trigonometry that

$$\cos\theta_{max} = \cos\eta/2 \, \cos\theta_{min} \, .$$

Thus for $\theta_{min} = 30°$, $\eta = 10°$, we find $\theta_{max} = 30.8°$, which is a good approximation to a constant θ for all events. By varying θ with η fixed at $10°$, we can then determine an angular distribution of ^{2}He particles $(d\sigma/d\Omega) \, (\theta)$ to be compared with predictions of DWBA calculations. The validity of this procedure is largely independent of our assumption about a two step process, but the absolute cross section would depend upon it through our ability to remove effects of the ^{2}He breakup from the measurements. It is convenient in these measurements to think of the elaborate detection system, involving time coincidence and energy summing to a fixed total, simply as a ^{2}He detector with some effective solid angle for detection which we determine from calculations. In this sense it measures $d\sigma/d\Omega$ for the (^{3}He,^{2}He) reaction.

II. EXPERIMENTAL

Foil targets of thickness ~1 mg/cm^2 were irradiated with a beam of 13 MeV ^{3}He nuclei from the University of Pittsburgh tandem Van de Graaff accelerator. Beam entered the 60 cm diameter scattering chamber through a circular aperture of 0.63 cm diameter. The target was centered in the chamber; the detection geometry is represented in Fig. 2. This figure displays the variables θ and η defined in Sec. I.

Contained in the chamber were an Ortec surface barrier detector of area 100 mm^2 and depth 2000 μm, and a Kevex lithium-drifted silicon (SiLi) detector of area 110 mm^2 and depth of 2000 μm; such detectors can stop protons of energy ~18 MeV. Measurements made for $\eta \leqslant 40°$ employed a holder used at 10 cm distance from target; those for $\eta \geqslant 40°$ were made at 3.5 cm distance. Thus high correlation angle measurements were characterized by greater solid angles of acceptance; angular positions at the 10 cm distance were defined to a full width of 6° in both θ and ϕ positions, with corresponding full widths of 10° in θ and 18° in ϕ for the 3.5 cm distance. Measurements made forward of $\theta = 90°$ employed $\eta = 10°$.

Exposures ranged in duration from a few minutes to ~2 hours, and beam currents ranged from a few nanoamps to ~400 nA, depending on target
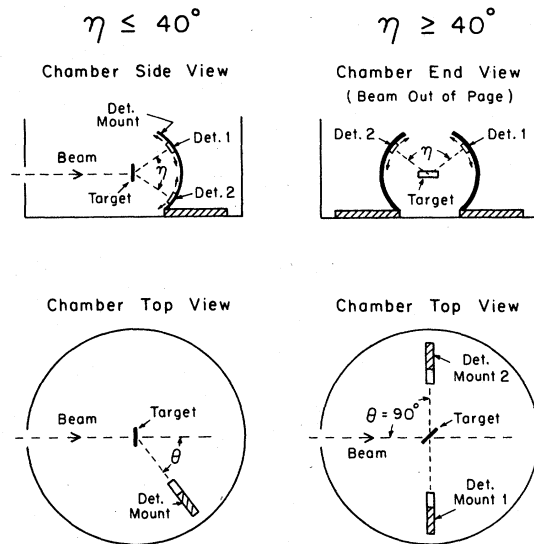

FIG. 2. Geometry of the experimental arrangement.

and geometry. Typical detector count rates were 15 000 to 20 000 cps; however, coincidence event rates were only 0.1 to 10 cps, so that pileup effects are not significant. Competition from (^{3}He,$p\alpha$) was investigated using particle identification techniques, and shown to be negligible. (^{3}He, dp) contributions are present in the data, but are energetically separable from (^{3}He, $2p$).

The circuitry employed is illustrated in Fig. 3. Each detector output is sent to a fast preamplifier (FPA), which outputs two pulses: a fast output to be used in timing circuitry, and a slow output for use with a charge sensitive preamplifier in energy circuitry. Typical timing peak widths were 10–15 ns. A coincidence event is characterized by three signals—one each for the respective energies E_1 and E_2 of the two coincident particles, and a time to amplitude converter (TAC) signal, characterizing the time separation of their detections. A slow coincidence of these signals triggers a multiplex acquisition of these three parameters (E_1, E_2, TAC) by an on-line acquisition program of the University of Pittsburgh Nuclear Physics
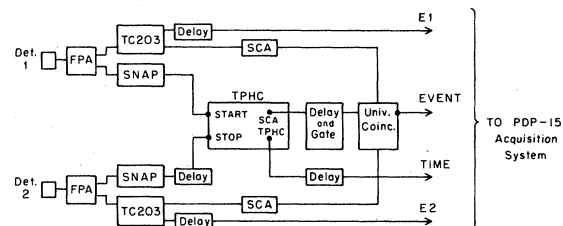

FIG. 3. Block diagram of electronic analysis system between the detectors and the computer.

Laboratory PDP-15 computer system.

The data are stored in disk memory by the addresses E_1, $E_1 + E_2$, TAC. Since each value of $E_1 + E_2$ corresponds to a unique excitation energy of the residual nucleus, a contour display of TAC vs $E_1 + E_2$ consists of clusters at values of $E_1 + E_2$ characteristic of excitation states of the residual nucleus. A two-dimensional window on such a display is then used to generate E_1 projections of the data, which are proportional to $d^3\sigma/d\Omega_1 d\Omega_2 dE_1$. This observable is to be compared to $P(E_1)$ generated from theory. Summing this data over E_1 (i.e., channel by channel) produces $d^2\sigma/d\Omega_1 d\Omega_2$ for the value of η of the experimental geometry. The shape of $(d^2\sigma/d\Omega_1 d\Omega_2)$ (η) is to be compared to $\int P(E_1)dE_1$ vs η, obtained from theory. Further, one can employ an effective solid angle, also obtained from theory, to extract from $d^2\sigma/d\Omega_1 d\Omega_2$ a value of $d\sigma/d\Omega$ for the (^{3}He, ^{2}He) reaction. This effective solid angle is calculated using the code CHIRP.

III. THEORY

A. Breakup simulation calculation

The (^{3}He, $2p$) reaction is viewed in two steps, as discussed in Sec. I. The first step is a neutron transfer, to be analyzed with DWBA calculations; the second step, ^{2}He breakup, is the subject of the simulation code CHIRP. Operationally, CHIRP yields three quantities:

(1) $P(E_1)$, the probability distribution in energy of protons observed by one detector, resulting from two proton coincidence events; $P(E_1)$ is to be compared to the shape of $d^3\sigma/d\Omega_1 d\Omega_2 dE_1$.

(2) $\int P(E_1)dE_1$ for various values of η. This angular correlation is to be compared to $(d^2\sigma/d\Omega_1 d\Omega_2)$ (η).

(3) An effective solid angle $\Delta\Omega_{eff}$, characteristic of the experimental system as a ^{2}He detector, to be used in experimental determination of $d\sigma/d\Omega$ for the (^{3}He, ^{2}He) reaction; $d\sigma/d\Omega$ is to be compared to predictions from DWBA calculations.

The approach is to view the ensemble of all possible ^{2}He breakup events, consistent with the conserved quantity $(E_1 + E_2)$ characteristic of the excitation state of the residual nucleus, as discussed in Sec. I. The method of the calculation is to establish grids in the various parameters required to describe a breakup event (see Fig. 4), and for each resulting event to follow the classical trajectories of the emitted protons, testing to see whether each proton is separately intercepted by one of the detectors in the experimental geometry under study, characterized by correlation angle η. The parameters specifying a breakup event are EBU, the energy of the two protons as observed from their center of mass, the geometrical variables ϕ and ψ required to specify the direction of the breakup relative to the two proton center of mass momentum, and α and β, the geometrical parameters necessary to specify the orientations of the detectors relative to the center of mass momentum. Further required
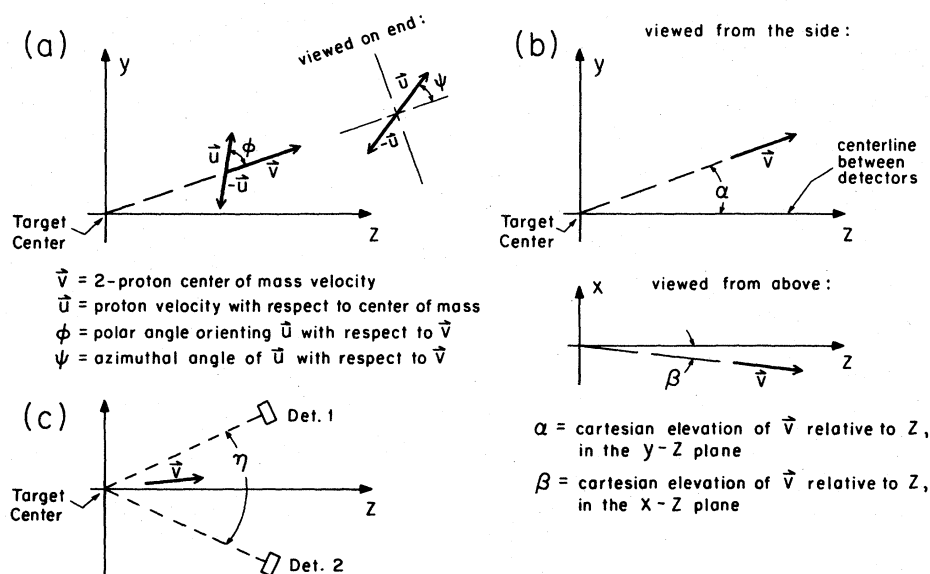

FIG. 4. Geometrical parameters specifying a ^{2}He breakup event: (a) relative orientation of the center of mass and breakup velocities; (b) relative orientation of the center of mass velocity and the Z axis defined as the line from the target to the center-line between the detectors; (c) side view from (b) including the detectors. Note that Z axis bisects the correlation angle η.

for the calculation are the dimensions of the detectors and their locations relative to the target. The velocities of the emergent protons are calculated according to the vector addition in Fig. 5.

For each breakup event resulting in detection of the two protons by the respective detectors, the kinetic energies E_1 and E_2 of the protons are computed and a properly normalized weighting proportional to

$$\sin\phi\, d\phi\, d\psi\ P(E_{BU})dE_{BU}$$

is added to running sums in energy bins corresponding to energies E_1 and E_2 in a 128-bin buffer covering approximately 18 MeV. The factor

$$\sin\phi\, d\phi\, d\psi$$

is the element of solid angle in the two proton center of mass frame, and reflects the assumption of isotropy of breakup directions in this frame. The factor

$$P(E_{BU})dE_{BU}$$

is the probability assigned to breakup at energy E_{BU}.

A basic kinematic restriction on the system is that only breakup energy E_{BU} less than or equal to the conserved quantity $E_1 + E_2$ need be considered. Further examination of the kinematics associated with Fig. 5 shows that for a particular correlation angle η, only a certain range of E_{BU} can contribute to detected events, as will be developed fully in Sec. IV. Thus, $(d^2\sigma/d\Omega_1 d\Omega_2)$ (η) measured for a particular region of η should be proportional to the average value of $P(E_{BU})$ for the corresponding region of E_{BU}.

After iteration over the full grids of the variables described above, the resulting entries in the energy buffer constitute the theoretical $P(E_1)$ distribution. Summing this quantity over E_1 then produces the $\int P(E_1)dE_1$; but this sum is also the fraction detected of all ^{2}He's emitted in a range of θ corresponding to the width of the detector centered about the observation angle ($\theta = 90°$ for the ^{64}Ni data), for the experimental geometry of correlation angle η. Then, multiplying this fraction

by the total solid angle intercepted by the detection system yields $\Delta\Omega_{eff}$, the effective solid angle for the experimental system in the η geometry, as a ^{2}He detector. This solid angle is then used in the usual manner to extract from the data experimental values of $(d\sigma/d\Omega)$ (θ) for the (^{3}He, ^{2}He) reaction.

B. DWBA calculations

Calculations of $(d\sigma/d\Omega)$ (θ) for the (^{3}He, ^{2}He) reaction employed code DWUCK, with the ^{2}He represented by a deuteron optical potential, and assuming charge of $+2$ and spin zero. Deuteron potentials for ^{64}Ni and ^{9}Be calculations were global potentials of Childs et al.[6]; ^{3}He potentials employed for ^{64}Ni were from Becchetti et al.[7] and for ^{9}Be were from Buffa et al.[8] The angular distributions calculated for ^{51}V, ^{65}Cu, and ^{89}Y employed Perey and Perey[9] optical parameters.

IV. DATA AND RESULTS ^{64}Ni(^{3}He,^{2}He) STUDIES AT $\theta = 90°$

A. Correlations between η and E_{BU}

An important element in understanding the results is the correlation between the energy in the ^{2}He breakup, E_{BU}, and the angle between the two emitted protons η. For E_{BU} less than $E_{2\,He}$, η is a maximum for a breakup direction perpendicular to the direction of ^{2}He motion; i.e., for $\phi = 90°$. Values of this maximum η as a function of E_{BU} are shown by the curve in Fig. 6. For $E_{BU} > E_{2\,He}$, η is a minimum for $\phi = 90°$, and this minimum η as a function of E_{BU} is also shown in Fig. 6. From these two it is clear that $\eta = 90°$ is a singular situation, and it is readily shown by simple geo-
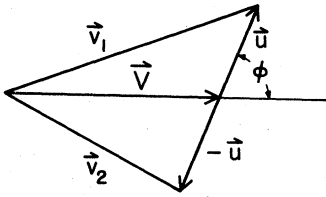
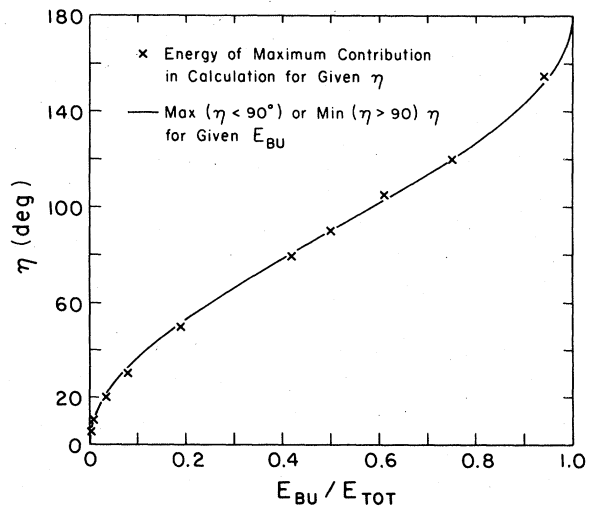FIG. 5. Breakup kinematics vector addition. $\vec{V}$, $\vec{u}$, ϕ are defined in Fig. 4, and $\vec{v}_1$, $\vec{v}_2$ are the resultant emergent velocities of the two protons in the laboratory system.

FIG. 6. Maximum or minimum η as a function of E_{BU} (curve); and value of E_{BU} contributing the maximum number of accepted events for a given η (crosses).

metrical arguments that $E_{BU} = E_{2\,He}$ is the necessary and sufficient condition for $\eta = 90°$.

Clearly solid angle considerations give a maximum weighting to the region near $\phi = 90°$, and this plus the fact that it is an extremum means that for a given E_{BU}, a large majority of the events occur with η close to the values shown by the curves in Fig. 6. This statement is more interesting if it is turned around—most of the events at a given η correspond to E_{BU} near the values shown by the curves in Fig. 6. However, this very interesting statement requires demonstration.

Such a demonstration is given in Fig. 7 which shows the relative contribution from each E_{BU} to CHIRP calculations for given values of η. We see that these are sharply peaked, and the positions of these peaks are plotted in Fig. 6 where it is evident that they fall very close to the curves. In view of the narrowness of the distributions in Fig. 7—note that the ordinate scale is logarithmic—it is a reasonably valid first approximation to say that there is a one-to-one correspondence between η and E_{BU} as shown by the points (and curves) in Fig. 6. This is an extremely useful approximation since the probability distribution of E_{BU}, $P(E_{BU})$ is a central factor in the theory which cannot be measured directly, whereas a probability distribution for η is directly measurable; in this approximation, the measured η distribution is equivalent to a measurement of the probability distribution for E_{BU}, $P(E_{BU})$. We next consider this matter.

B. Angular correlation between emitted protons

The angular correlation between the emitted protons in the reaction ^{64}Ni (^3He, ^2He) leading to the ground state of ^{65}Ni with $\theta = 90°$ is shown in Fig. 8, where for present purposes the ordinate may be considered to be the relative intensity as a function of η. Also shown in Fig. 8 are the angular correlations calculated by the CHIRP code for P-G-B and W-M final state interactions. We see there a large discrepancy between theory and experiment in that the experimental angular correlation falls off much more rapidly with increasing η for angles beyond 30°.

Because of the close relationship between η and E_{BU} discussed in the last section, it is easy to find a $P(E_{BU})$ function that greatly improves the fit in Fig. 8. A first approximation is to take the relationship in Fig. 6 as a one-to-one correspondence; for example, in Fig. 8 the point at $\eta = 60°$ is lower than the theoretical prediction by a factor of 3.3, and in Fig. 6 $\eta = 60°$ corresponds to $E_{BU} = 0.25\,E_{tot}$, so we reduce $P(E_{BU})$ for this E_{BU} relative to the original value by a factor of 3.3 With the $P(E_{BU})$ function thereby obtained, we calculated a new η angular distribution. This is the first step in a pertur-
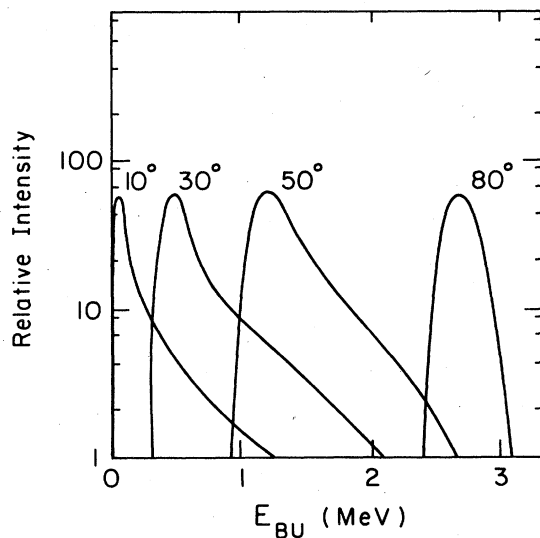

FIG. 7. Relative contribution of each E_{BU} to the accepted events for a given η. The maxima of these curves are shown by the crosses in Fig. 6.
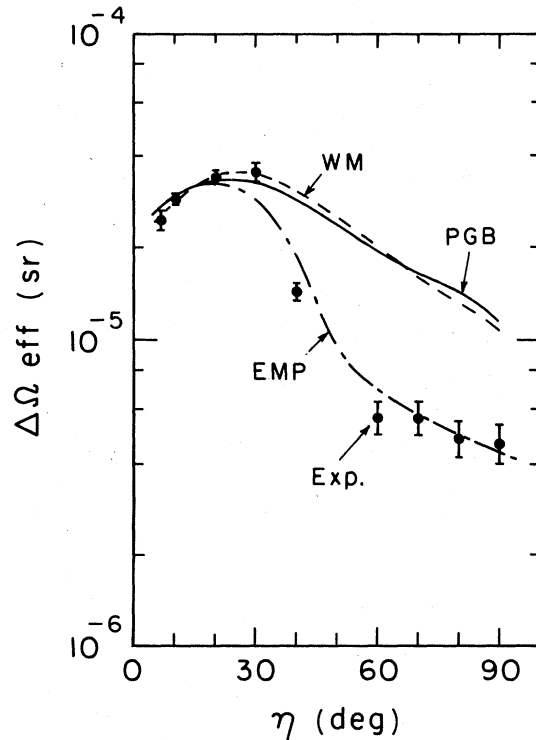

FIG. 8. Relative number of accepted events as a function of η from experiment (points with error bars), and from calculations using various final state interactions.

bation program that may be repeated as often as desired, but actually there was little improvement after the above described first perturbation. The final state interaction obtained after two perturbations is shown in Fig. 9—we refer to it hereafter as EMP for "empirical"—and the η angular distribution obtained from it is shown by the dot-dash curve in Fig. 8. It is clearly impossible to reproduce the very sharp drop in the data between 30° and 40°, with a smoothly varying final state interaction, but if this is regarded as an experimental fluctuation, the fit in Fig. 8 is quite good.

The final state interaction required to get this fit, shown in Fig. 9, is a very sharply peaked one, with a peak near $E_{BU} = 0.5$ MeV and a full width at half maximum of about 0.6 MeV. It would be easy to jump to the conclusion that this is a resonance in the p-p system unbound by 0.5 MeV, which is in good agreement with a crude estimate of the energy of the isobaric analog state of the singlet deuteron corrected for the Coulomb energy; however, such speculation is severely limited by the fact that the P-G-B and W-M final state interactions are derived from the p-p interaction accurately known from measurements of elementary particle p-p scattering. Further consideration of the meaning of our empirical final
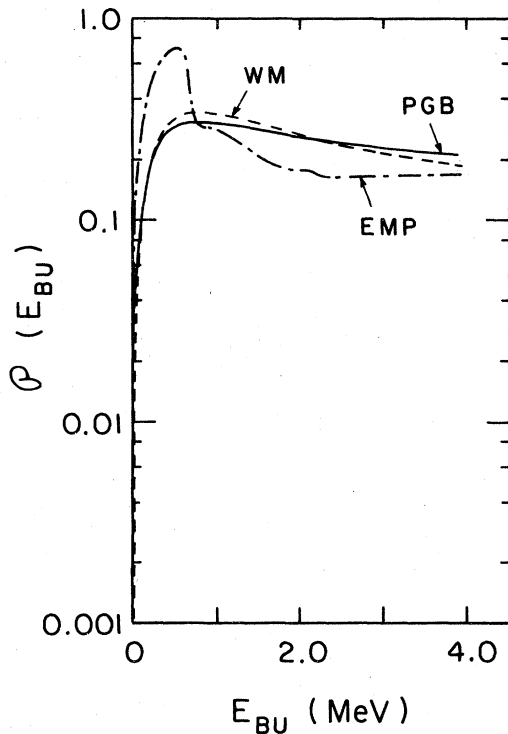
state interaction is beyond the scope of this paper.

Our empirical final state interaction bears a striking resemblance to one reported by Gavron[10] from measurements of (^{3}He, $2p$) reactions on ^{208}Pb with 25 MeV ^{3}He ions using a highly unconventional detection technique. His result was a final state interaction peaked sharply at 0.3 MeV with a full width at half maximum of only 0.3 MeV. on the other hand, Simpson et al.[11] and Niiler et al.[12] reported successful use of the PGB final state interaction in analyzing ^{2}H(p, $2p$)n reactions; they implied that their work was a verification of that interaction. The failure of PGB in Fig. 8 must be interpreted as a strong contradiction of their conclusions

Proton angular correlations in the ^{64}Ni (^{3}He, ^{2}He) reaction leading to excited final states in ^{65}Ni are shown in Fig. 10, where they are compared with corresponding results for transitions to the ground state. We see that there is a great deal of similarity in the results for the various transitions. There is no difficulty in applying the same theoretical treatment, and the conclusions are the same as for the ground state transition.

Also shown in Fig. 10 is the angular correlation for the (^{3}He, pd) reaction leaving ^{64}Ni in its ground state, and it is evident that it is very different from those for (^{3}He, ^{2}He). However, it also has the sharp drop from 30° to 40°, which indicates that that sharp drop in the (^{3}He, ^{2}He) angular correlations may be partly of experimental origin.

C. Energy spectra at a given η

A typical experimental energy spectrum is shown in Fig. 11. Data of this type are fitted to
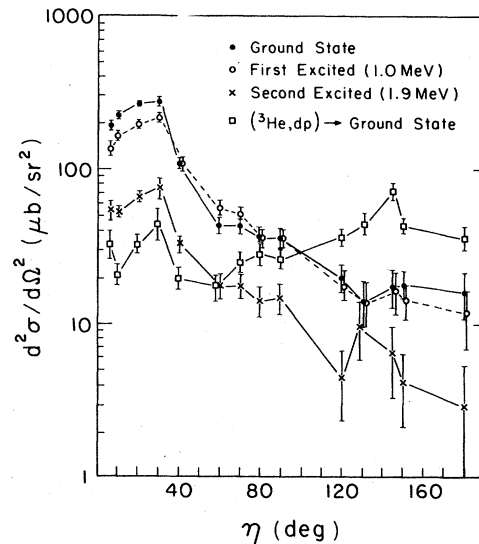

FIG. 9. Final state interaction from empirical fit compared to those in Fig. 1.

FIG. 10. Proton angular correlations from the ^{64}Ni(^{3}He,^{2}He) reaction leading to excited final states in ^{65}Ni.

a smooth curve constrained to be symmetrical about the midpoint energy as in Fig. 11, and it is these curves which we now discuss.

The energy spectra of protons from transitions leading to the ground state of ^{65}Ni in the reaction ^{64}Ni (^{3}He, ^{2}He) are shown in Fig. 12 for various angles, η, between the two emitted ptotons, and calculations of these with the CHIRP code are also shown.

The most striking feature in the data is the dip in the center of the spectrum for small η with its depth decreasing rapidly as η increases, and it is most gratifying to see this feature reproduced in the theoretical calculations. For a given η, the center of the spectrum corresponds to $\phi = 90°$ and E_{BU} a minimum; for very small E_{BU}, the $P(E_{BU})$ function decreases very rapidly with decreasing E_{BU}, which suppresses the contribution of the minimum E_{BU} and hence causes a dip at the center of the spectrum. The rate of decrease with decreasing E_{BU} is greater for the W-M than for the P-G-B final state interaction, which explains why the central dips are deeper for that case.

One discrepancy between theory and experiment in Fig. 12 is that the theoretical curves appear to be broader than the experimental and this difference increases with increasing η. Actually the width of the theoretical spectra can be adjusted by selection of the Coulomb energy; in the calculations shown the latter was chosen to fit the width of the measured spectra at about 0.003 of maximum with the very important constraint that only a single Coulomb energy is used for data
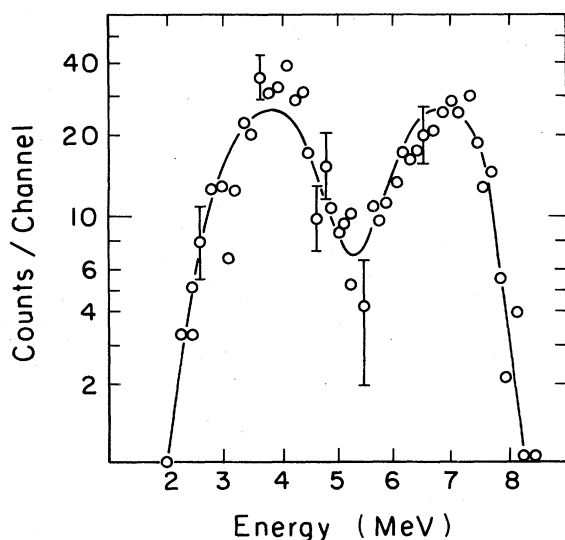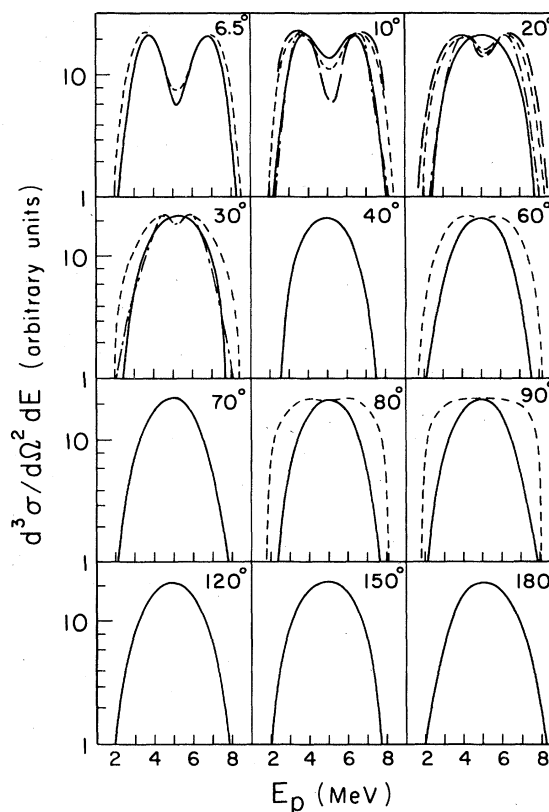

FIG. 12. Energy spectra of protons from transitions leading to the ground state of ^{65}Ni in the ^{64}Ni(^{3}He,^{2}He) reaction with various values of η (shown in top right corner). Solid lines are experimental. Short dash, long dash, and dot-dash lines show theoretical predictions for Phillips-Griffy-Biedenharn, Watson-Migdal, and empirical final state interactions, respectively.

at all angles from a given target. Thus the discrepancy under discussion is actually in the *slope* of the sides of the spectra; these are steeper in the PGB calculations than in the measurements. This discrepancy seems to be largely eliminated if the empirical final state interaction EMP from Fig. 9 is used. For large angles such as 80°, the empirical final state interaction is not well determined in the relevant region of E_{BU}, so it is not very meaningful to make comparisons with experimental spectra. In any case, the cross section is so small at these η values that competing reaction mechanisms may have important effects.

The other discrepancy between theory and experiment in Fig. 12 is that the central dips in the spectra extend to higher η values in the theoretical curves than in the experimental ones. It is difficult to understand the reason for this; our understanding of the central dips expressed above would predict that it should disappear for η cor-

FIG. 11. Typical data on distribution of energies E_1. These data are for transitions to the ground state in ^{64}Ni(^{3}He,^{2}He) reactions with $\eta = 6.5°$.

responding to E_{BU} in Fig. 6 beyond the maximum in the $P(E_{BU})$ curve, which would be at $\eta \simeq 25°$. It would not be difficult to understand why the central dips should disappear at smaller angles than this, as the slope of the $P(E_{BU})$ curves is relatively small for E_{BU} corresponding to $\eta > 15°$ in Fig. 6, but it is difficult to understand persistence of the central dip beyond 25°. Thus our expectations for the theory were closer to the experimental results than to the curves calculated from theory.

A few energy spectra from the ^{64}Ni (^{3}He, ^{2}He) reaction exciting the first cluster of excited states in ^{65}Ni are shown in Fig. 13 along with spectra at the same η from Fig. 12 for exciting the ground state cluster. We see that aside from the expected shift in energy, the features of the spectra are essentially identical.

D. Cross section

Using the treatment given in Sec. III, an effective solid angle for ^{2}He detection can be calculated for each η and used to derive experimental values for $d\sigma/d\Omega$ for the (^{3}He, ^{2}He) reaction. The result for excitation of the ground state cluster is $d\sigma/d\Omega = 0.53$ mb/sr at $\theta = 90°$.

This result may be compared directly with predictions of DWBA calculations. The nuclear states involved are $E^* = 0$, $f_{5/2}$; $E^* = 0.062$ MeV, $p_{1/2}$; and $E^* = 0.309$ MeV, $p_{3/2}$. The spectroscopic factors for exciting these states are known from studies of (d,p) reactions,[13] and using them the DWBA calculations gives $d\sigma/d\Omega(90°) = 0.35$, 0.90, and 0.12 mb/sr, respectively, for a total $d\sigma/d\Omega = 1.37$ mb/sr for the entire cluster.

The discrepancy between the measured value 0.53 mb/sr and the theoretical prediction 1.37 mb/sr is probably not larger than might be expected from the facts that a deuteron nuclear wave function was used for the ^{2}He in the DWBA calculation and the normalization factor for the

(^{3}He, ^{2}He) reaction is not well known. In the calculations discussed above, this normalization was assigned the value for the (^{3}He, d) reaction, viz., 4.42. Moreover, $\theta = 90°$ is a large angle compared to the angular region in which DWBA calculations are expected to work well in predicting absolute cross sections. The fact that the experimental and theoretical cross sections are not grossly different contributes somewhat to our confidence that the reaction mechanism is indeed (^{3}He, ^{2}He).

A somewhat more quantitative test is available in the ratio of cross sections for exciting various states of ^{65}Ni in these reactions. In this ratio, uncertainties in the determination of effective solid angles essentially cancel out, as do the uncertainties in the DWBA normalization factor. The ratio of cross sections for excitation of the first excited (1.0 MeV) cluster to the ground state cluster is 0.78 in the experiment (cf. Fig. 10) vs 1.06 in the DWBA calculation. In view of the inclusion of several nuclear states with different angular momentum transfers in each cluster, this is reasonably good agreement.

The ratio of cross sections for excitation of the second excited (1.9 MeV) cluster to the ground state cluster is 0.28 in the experiment vs 0.55 in the DWBA calculation. This factor of 2 discrepancy is somewhat disappointing but in view of the unfavorable energetics and large Coulomb effects, it is not too difficult to explain.

V. DATA AND RESULTS—OTHER TARGETS AND θ VALUES

A. Other targets at $\theta = 90°$

Studies were made using the techniques discussed above for six other target nuclei spread through the mass range up to $A \sim 100$, which is about the heaviest mass at which good measurements could be made with 13 MeV bombarding energies. Energy distributions for $\eta = 10°$ and a few higher values are shown in Figs. 14 and 15. We see that the results are quite similar to those for ^{64}Ni shown in Fig. 12 in that there is a central dip for $\eta = 10°$ but not for $\eta \geq 20°$, and the experimental angular distributions are somewhat narrower than predicted by the PGB theory. The central dips are somewhat deeper for the lighter target nuclei, but this can be understood as a consequence of their lower Coulomb energy and hence wider range of energies available; for Al, the Coulomb energy is 1 MeV allowing proton energies over the range 1–10 MeV, whereas for Zr the Coulomb energy is 3 MeV allowing proton energies only over the range 3–8 MeV. There are small variations in the ratio of peak heights for $\eta = 10°$ and $\eta = 30°$; it is close to unity for the lightest element
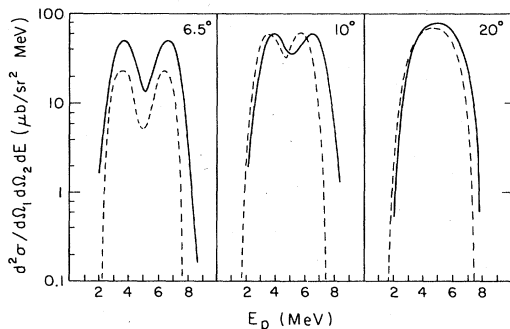

FIG. 13. Measured energy spectra of protons from ^{64}Ni(^{3}He,^{2}He) reactions exciting the first excited cluster of states (solid) compared with those exciting the ground state cluster from Fig. 11 (dashed).
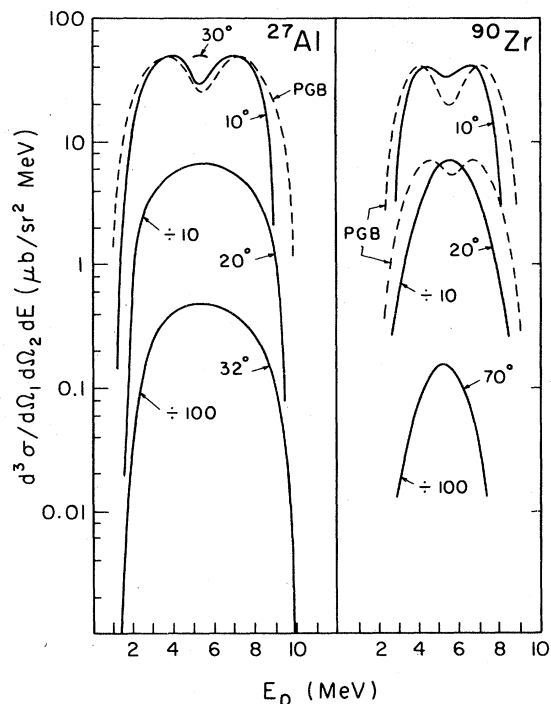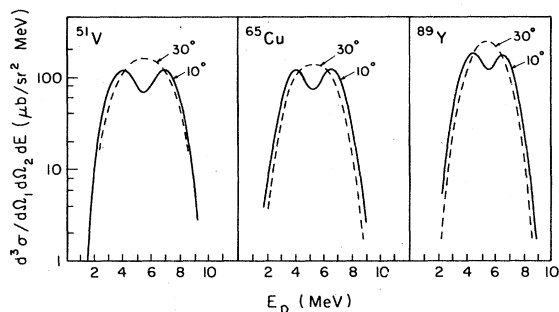
FIG. 14. Measured energy spectra of protons from (^{3}He,^{2}He) reactions on the targets shown, with values of η attached to curves. Dashed curves show theoretical predictions using the P-G-B final state interaction.

(Al) and it rises to 1.3 for the heaviest. This is probably also explainable by the difference in the available energy range.

In general, then, there is no reason to believe that the considerations of the last section do not apply to target nuclei of all masses.

B. Angular distributions of ^{2}He

One spin-off of the work reported here is that it is an important step toward development of a ^{2}He detector which may then be used as a tool for studying nuclear reactions in which ^{2}He particles

FIG. 15. Measured energy spectra of protons from (^{3}He,^{2}He) reactions on the targets shown, with values of η attached to curves.
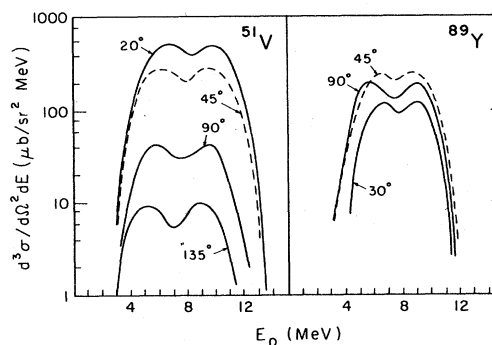

FIG. 16. Measured energy distributions for protons from (^{3}He,^{2}He) reactions with $\eta = 10°$ and θ values attached to curves.

are emitted. A typical study of this type might be a measurement of angular distributions of ^{2}He from (^{3}He, ^{2}He) reactions, that is, a measurement of the θ distribution of ^{2}He emission. We now address that subject.

There are important advantages of using $\eta \sim 10°$ in such a detector:

(1) The central dip in the spectrum gives a clear signal that ^{2}He particles are being detected, and other (^{3}He, 2p) processes are not important con-
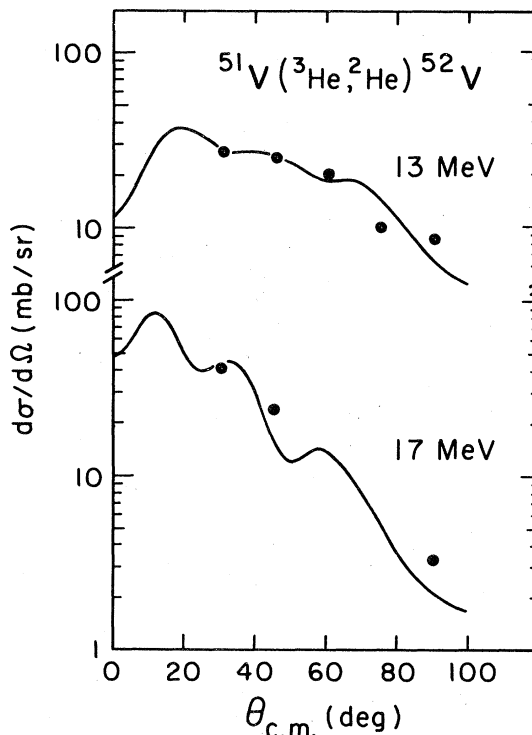

FIG. 17. Angular distribution of ^{2}He from (^{3}He,^{2}He) reactions induced by 13 MeV and 17 MeV ^{3}He particles incident on a ^{51}V target and exciting states near the ground state. Curves show DWBA calculations.
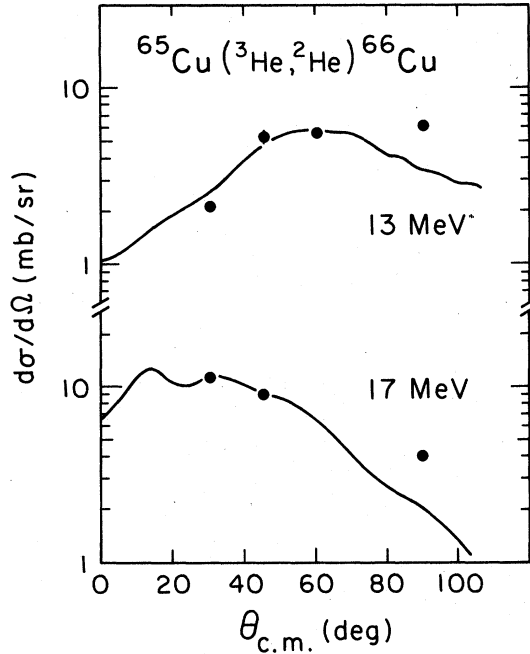
FIG. 18. Angular distribution of ^{2}He from (^{3}He,^{2}He) reactions induced by 13 MeV and 17 MeV ^{3}He particles incident on a ^{65}Cu target and exciting states near the ground state. Curves show DWBA calculations.
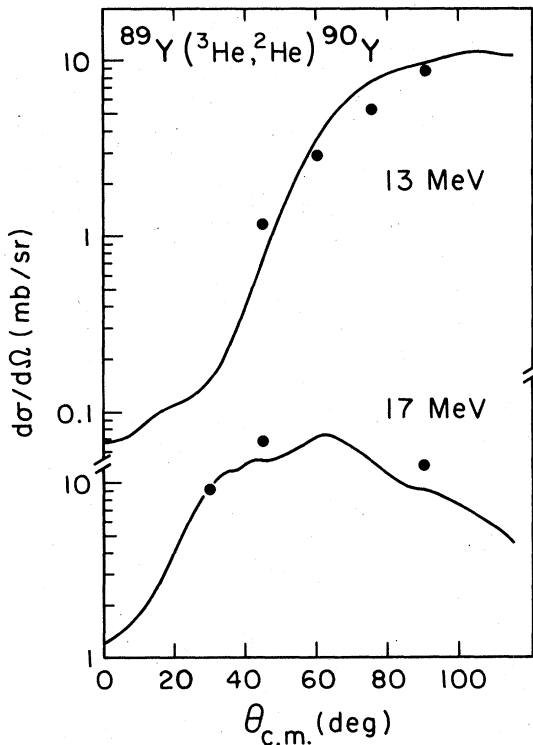
FIG. 19. Angular distribution of ^{2}He from (^{3}He,^{2}He) reactions induced by 13 MeV and 17 MeV ^{3}He particles incident on a ^{89}Y target and exciting states near the ground state. Curves show DWBA calculations.
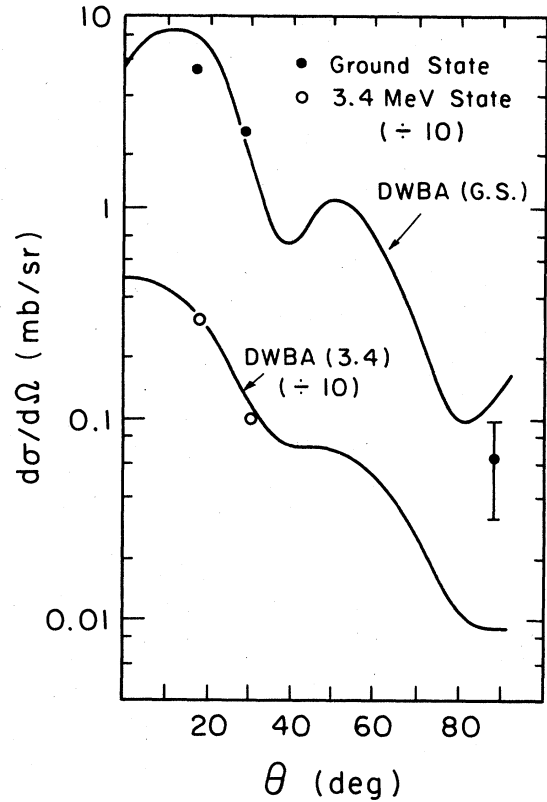
FIG. 20. Angular distribution of ^{2}He from (^{3}He,^{2}He) reactions induced by 13 MeV ^{3}He on a ^{9}Be target and exciting the ground state and 3.4 MeV excited state of ^{10}Be. Curves show DWBA calculations.

tributors.

(2) Only when $\eta \ll \theta$ is the angle θ well defined in the experiment.

(3) Efficiency of the detector is near the maximum (cf. Fig. 10).

An argument could be made for using an annular detector to obtain a smaller η, but this would have required an appreciable extra expense. Since $\eta = 10°$ seemed adequate, it was the one chosen.

It was also decided to make measurements at two bombarding energies, and 17 MeV was chosen as the additional energy to be used. The energy distributions for $\eta = 10°$ and various θ are shown for a relatively light and a relatively heavy target in Fig. 16. We see that they are very much as expected, including the central dip. The slight energy shifts are explainable as rising from the reaction kinematics.

Crude angular distributions were measured for three of the targets with both 13 and 17 MeV bombarding energy and the results are shown in Figs. 17, 18, and 19, where they are compared with DWBA predictions employing a (^{3}He, ^{2}He) normal-

ization factor of 10, chosen to fit the measured intensity. We see there that the agreement is quite satisfactory. In particular, the trends in the angular distributions are well reproduced, including their variation with bombarding energy and with target mass. The differences in the ^{89}Y data between the two bombarding energies are somewhat spectacular, but they are still well reproduced.

While the primary interest in this work is on heavy nuclei, it was considered worthwhile to check on its applicability to light nuclei. Data for ^{9}Be(^{3}He, ^{2}He) exciting the ground state and first excited (3.4 MeV) state of ^{10}Be are shown in Fig. 20 where they are compared with DWBA predictions; here too, a (^{3}He, ^{2}He) normalization factor of 10 has been employed in the predictions. We see that within the limits of the sparsity of the data, the agreement is reasonable. Note that the cross section is very small at angles as large as 90°.

From these results it may be concluded that the method used would be useful for measuring angular distributions of ^{2}He particles from nuclear reactions. Recent work reported by Van Driel et al.[14] on (^{3}He, ^{2}He) reactions corroborates and demonstrates this conclusion.

[1]R. E. Brown, J. S. Blair, D. Bodansky, N. Cue, and C. D. Kavaloski, Phys. Rev. 138, B1394 (1965).

[2]B. L. Cohen, E. C. May, and T. M. O'Keefe, Phys. Rev. Lett. 18, 962 (1967); B. L. Cohen, E. C. May, T. M. O'Keefe, and C. L. Fink, Phys. Rev. 179, 962 (1969).

[3]K. M. Watson, Phys. Rev. 85, 1163 (1952).

[4]A. B. Migdal, Zh. Eksp. Teor. Fiz. 28, 3 (1955) [Sov. Phys.—JETP 1, 2 (1955)].

[5]G. C. Phillips, T. A. Griffy, and L. C. Biedenharn, Nucl. Phys. 21, 327 (1960).

[6]J. D. Childs, Ph.D. thesis, Univ. of Pittsburgh, 1976 (unpublished).

[7]F. D. Becchetti, W. Makofske, and G. W. Greenlees, Nucl. Phys. A190, 437 (1972).

[8]A. J. Buffa, Jr. and M. K. Brussel, Nucl. Phys. A195, 545 (1972).

[9]C. M. Perey and F. G. Perey, Phys. Rev. 134, B353 (1964).

[10]A. Gavron, Phys. Rev. C 13, 98 (1976).

[11]W. D. Simpson, W. R. Jackson, and G. C. Phillips, Nucl. Phys. A163, 97 (1967).

[12]A. Niiler, C. Joseph, V. Valkovic, W. von Witsch, and G. C. Phillips, Phys. Rev. 182, 1083 (1969).

[13]R. L. Auble, Nucl. Data Sheets 12, 305 (1974).

[14]J. Van Driel, R. K. Kamermans, R. J. de Meijer, and A. E. L. Dieperink, Nucl. Phys. A342, 1 (1980).